Journal of Power Sources 222 (2013) 210–217

Contents lists available at SciVerse ScienceDirect

Journal of Power Sources

journal homepage: www.elsevier.com/locate/jpowsour

A nonlinear equivalent circuit model for lithium ion cells

Krishnan S. Hariharan*,[1], V. Senthil Kumar [1]

India Science Lab, General Motors Global R & D, Creator Building, International Technology Park, Whitefield Road, Bangalore 560066, India

HIGHLIGHTS

- Nonlinear equivalent circuit model for lithium ion cells.
- The circuit elements are based on charge transfer reaction and variable resistances.
- The potential drops are the natural state variables rather than cell state-of-charge.
- A pulse protocol was predicted accurately within an error of 50 mV.
- Voltage predicted without parameter re-estimation, amenable as an on-board algorithm.

ARTICLE INFO

Article history:
Received 18 June 2012
Received in revised form
26 August 2012
Accepted 27 August 2012
Available online 7 September 2012

Keywords:
Lithium ion battery
Nonlinear equivalent circuit model
Voltage based variable resistances
Battery management system

ABSTRACT

A nonlinear equivalent circuit model for lithium ion cells is developed where the circuit elements are based on electrochemical processes like charge transfer reaction, and variable resistances that are functions of the state variables. The potential drops are the natural state variables rather than cell state-of-charge (SOC). A commercial pouch cell consisting of composite positive and meso-carbon microbeads (MCMB) negative electrodes is analyzed. The state space model developed consists of the current balance which forms the state variable evolution equation and voltage balance which forms the output equation. The global set of parameters for a two pair resistor–capacitor circuit is calculated by solving the model equations consistently and minimizing the error with HPPC (Hybrid Pulse Power Characterization) pulse voltage at few SOCs. The entire HPPC protocol is predicted by the model accurately within an error of 50 mV. The model is validated using the full depth charge–discharge experiments. The model is used to resolve the overall cell potential into potential drops due to individual processes, yielding insights into controlling mechanisms. The variable resistor formalism enables cell voltage prediction without parameter re-estimation and hence can be developed as an on-board algorithm.

1. Introduction

The lithium ion battery technology has been proven as an alternate energy source in electric vehicle or hybrid electric vehicle applications due to its high energy density, light weight, low self-discharge and other features [1]. To exploit the advantages of different lithium compounds, recent positive electrode compositions consider multiple active materials. Although the technology has proven successful [2], and there are modeling efforts from an electrochemical approach [3], an accurate model that can be used as a predictive and on-board tool that represents various cell processes of a commercial cell is still wanting.

Equivalent electric circuit representations for cells [4,5] have received much importance due to the conceptual simplicity that enables the models to be integrated with control algorithms at a system level, and is potentially suitable for on-board applications in an automobile. The pertinent variables do not have spatial dependence, and the model equations based on electrical circuit theory are solved as a set of ordinary differential equations (ODEs). An equivalent circuit model should be robust, accurate over a wide range of operating conditions, and easy to compute.

The equivalent circuit model equations can be formulated and solved either in the time domain or in the frequency domain. In the time domain formulation, although the models are successful in representing the cell charge–discharge data, most of the approaches are purely empirical. A direct connection of the

* Corresponding author. Tel.: +91 80 4201 2749; fax: +91 80 4115 8262.
E-mail address: krishnan.sh@gmail.com (K.S. Hariharan).
[1] Present address: Samsung Advanced Institute of Technology, SISO Pvt. Ltd., Bangalore 560093, India.

0378-7753/$ – see front matter © 2012 Elsevier B.V. All rights reserved.
http://dx.doi.org/10.1016/j.jpowsour.2012.08.090

parameters with the electrochemical processes is seldom attempted restricting the predictability of the model. The equations are often linearized and solved as difference equations, and the parameters are estimated at every solution time step. This solution procedure results in a large number of uncorrelated parameters, which often lead to unphysical values that depend on the time step used in the solution method. The model parameters are reported in terms of a system variable [6,7], typically the cell state-of-charge (SOC). The functional dependence is typically built-in posteriori and ad hoc.

In the frequency domain formulation, the physical basis of the parameters is sought predominantly through impedance analysis [8]. Impedance analysis is conducted around an equilibrium state and parameters so obtained cannot be used directly to non-equilibrium scenarios like constant power or constant current or pulse cell charge–discharge data. Hence, there are only a few approaches where impedance spectrum [9–13] is used to predict the discharge behavior of commercial cells. In the present work, a time domain formulation of the equivalent circuit model with physics-based functional forms for the model parameters is proposed.

The state space approach represents the state of the system using a minimal set of state variables. Each state variable is obtained by solving its own evolution equation, and the remaining process variables are obtained from the state variables. The state space approach is used extensively in the control systems theory and is amenable for large scale system simulations as in vehicle models. State space models are applied to equivalent circuit cell models predominantly in association with a Kalman filter algorithm, thus making the solution scheme inherently discrete in time [14], with varying parameter values. This approach is used to estimate the equilibrium potential V_0 and the corresponding SOC [15–19] leading to various SOC estimation algorithms [20] applied to drive profiles [21]. The state space approach in conjunction with Kalman filter algorithm is also used with the electrochemical model [22–24].

An approach that combines the mathematical simplicity of the equivalent circuit model and the rigor of the state space approach, with functional forms of parameters from electrochemical or physical processes, would result in numerically robust models. Such models could be used to obtain insights into the controlling processes and potentially be used as a predictive or a design tool, in addition to a characterization tool.

In this work a nonlinear equivalent electric circuit model for a commercial cell is developed. The zero current regime of the HPPC (hybrid pulse power characterization, explained later) data is analyzed to establish the adequate circuit to be used. A general equation for an N pair RC is derived, and analytical solutions for special cases obtained. The key step of identification of the state variables is done by analysis of the electrochemical processes. The electric circuit thus considered in this work consists of elements that represent the Butler–Volmer reaction and nonlinear variable resistances. It is observed that the overpotential, or the potential drops across the circuit elements are the natural state variables rather than the cell state-of-charge. It is to be noted that the effects of overpotential on cell processes have not been studied in detail till recently [25]. This formulation enables a direct solution procedure, reduces the number of parameters and empiricism. The parameters are estimated by minimizing the error between the model output and the HPPC data at select SOCs. The predictability of the model is demonstrated at other SOCs as well as the entire HPPC protocol. The model is validated using full depth charge–discharge data that includes Ragone (constant power) and constant current charge–discharge data.

2. *N* pair *RC* equivalent circuit model development

The equivalent circuit approach represents the cell in terms of electric circuit elements that corresponds to the ionic or electronic flow in the cell. The various processes are identified and modeled using resistors (R), capacitors (C) and its generalizations (Constant Phase Element or CPE) [9], and in rare cases inductors. The most general representation that arises from electrochemical impedance spectrum of the cell is that of a sequence of RC (R is parallel to C) or R-CPE circuits with a Warburg element representing diffusion [9,10]. However, this circuit does not have a direct solution in the time domain. As the present approach is to model the time domain data, simplifications of this model are sought, without sacrificing the electrochemical basis of the parameters. A simplification that has been successful is to consider the circuit as consisting of a fixed number of RC elements, the generalization being an N pair RC (Fig. 1).

2.1. Overall voltage balance and individual RC pair current balance

The voltage balance for the cell, represented by an N pairs of RC circuits, where the cell voltage V is related to the equilibrium potential V_0, the voltage drop across the resistor due to the current I and resistance R, and the voltage drop across the nth RC pair, V_n, is

$$V = V_0 + IR + \sum_{n=1}^{N} V_n \tag{1}$$

The current balance for the nth pair RC is

$$I = I_{C_n} + I_{R_n}, \tag{2}$$

where the current through the capacitor is

$$I_{C_n} = \frac{dQ_n}{dt}, \tag{3}$$

with $Q_n = V_n \cdot C_n$, and the current through the resistor is

$$I_{R_n} = \frac{V_n}{R_n} \tag{4}$$

Substituting these expressions in Eq. (2) the current balance is

$$I = \frac{d}{dt}[C_n V_n] + \frac{V_n}{R_n} \tag{5}$$

Equation (5) is applied to all the RC pairs in the circuit. Thus the system is a set of N ordinary differential equations (ODEs) involving the voltage drops across individual pairs of RCs and the voltage balance for the cell, Eq. (1). It is interesting to note that the

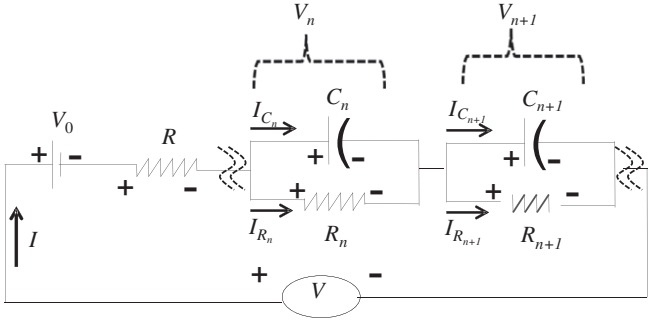

Fig. 1. The N pair RC model.

equilibrium potential appears only in the overall voltage balance (Eq. (1)) and not in the current balances of the individual *RC* pairs (Eq. (5)). The set of equations can be solved once the initial value for all the V_n is specified.

2.2. Initial values of the RC pair voltage drops

When cell is at equilibrium, the capacitors are fully discharged. When current flow starts, initially the current flows only through the capacitor [5] and not through the resistor. Hence, the circuit simplifies to *N* capacitors in series. For such a circuit, the charge accumulated in each capacitor is identical. And hence, the ratio of initial voltage drops is inversely proportional to the ratio of capacitances i.e.

$$Q_n(0) = Q_{n+1}(0) \tag{6}$$

$$V_n(0)C_n = V_{n+1}(0)C_{n+1} \tag{7}$$

$$\frac{V_n(0)}{V_{n+1}(0)} = \frac{C_{n+1}}{C_n} \tag{8}$$

At $t = 0$, using Eq. (8), Eq. (1) can be written as

$$V(0) - V_0(0) - I(0)R = \sum_n V_n(0) = V_n(0)\sum_m \frac{V_m(0)}{V_n(0)} = V_n(0)\sum_m \frac{C_n}{C_m} \tag{9}$$

Rearranging for the initial voltage drop gives

$$V_n(0) = \left[\frac{V(0) - V_0(0) - I(0)R}{C_n \sum_m \frac{1}{C_m}}\right] \tag{10}$$

With these initial voltage drops, the current balance equations for the individual *RC* pairs Eq. (5) can be solved. The cell voltage is then obtained from Eq. (1).

3. Identification of the minimal equivalent circuit

The actual number of *RC* pairs required to describe a cell response should ideally be determined from an experimental impedance analysis. For example, the charge transfer reaction is either modeled using a single *RC* pair or a more general R-CPE pair [9–13]. In the absence of degradation processes, the main process apart from reaction is solid phase diffusion, which is typically modeled using a Warburg element in series with the reaction resistance. One simplification is to bring the Warburg element to the main limb of the equivalent circuit as seen in Refs. [9,10]. In the time domain, the Warburg element can be represented as a series of *RC* pairs [9]. As a limiting case, it could be represented by a single *RC* pair. Thus one could model the reaction–diffusion processes in a cell minimally with a 2 pair *RC* circuit. Note that the minimal circuit required to describe a cell response could change with operating conditions, or aging. For example, at very low temperatures, there could be additional resistances building up due to freezing of electrolyte, extremely slow solid diffusion etc. requiring additional elements in the equivalent circuit.

When the external current of the cell is switched off, the voltage drop due to electronic, ionic and contact resistances vanish, and the processes like the charge transfer reaction and the solid phase diffusion relax to their equilibrium states. The relaxation process can be observed as the change in the cell voltage as it reaches V_0. Thus the rest data enables one to study the reaction–diffusion processes in the absence of external driving forces. Hence voltage relaxation during rest period can be used to identify the minimal number of *RC* pairs in an equivalent circuit required to adequately describe the underlying reaction–diffusion processes. Under a constant current operation one can obtain analytical solutions for the cell voltage. For a two pair *RC*, cell voltage is given by solving Eqs. (1) and (5) as

$$V = V_0 + IR + IR_1\left[1 - \exp\left(\frac{-t}{R_1C_1}\right)\right] + IR_2\left[1 - \exp\left(\frac{-t}{R_2C_2}\right)\right] + V_1(0)\exp\left(\frac{-t}{R_1C_1}\right) + V_2(0)\exp\left(\frac{-t}{R_2C_2}\right) \tag{11}$$

During rest phase, Eq. (11) reduces to

$$V = V_0 + V_1(0)\exp\left(\frac{-t}{R_1C_1}\right) + V_2(0)\exp\left(\frac{-t}{R_2C_2}\right); \tag{12}$$

In Fig. 2, we have fitted the 2 pair *RC* equation, Eq. (12), to voltage during rest region of the HPPC, and it is seen that the 2 pair *RC* model fits the data much more accurately than a one pair *RC* model. These results indicate that the cell response requires at least a two pair *RC* for complete representation, and hence has been used in all further analysis.

4. Equivalent resistance of the charge transfer reaction

In the 2 pair *RC* circuit, let R_1 represent the charge transfer reaction. Note that there are charge transfer reactions occurring both in anode and cathode. Typically one of them is expected to be controlling and R_1 represents it. The charge transfer current is represented by the Butler–Volmer equation [26] that relates the current generated to the overpotential and the concentrations

$$i = FKC^{\alpha_a}\left(C_{s,\max} - C_{s,R_p}\right)^{\alpha_a} C_{s,R_p}^{\alpha_c}\left[\exp\left(\frac{\alpha_a F(\phi_1 - \phi_2 - V_0)}{R_G T}\right) - \exp\left(-\frac{(1-\alpha_c)F(\phi_1 - \phi_2 - V_0)}{R_G T}\right)\right] \tag{13}$$

where ϕ_1 and ϕ_2 are the solid and liquid phase potentials of an electrode, the overpotential is given by $(\phi_1 - \phi_2 - V_0)$; *K* the rate constant, C_{s,R_p} and $C_{s,\max}$ are the solid concentrations at the surface

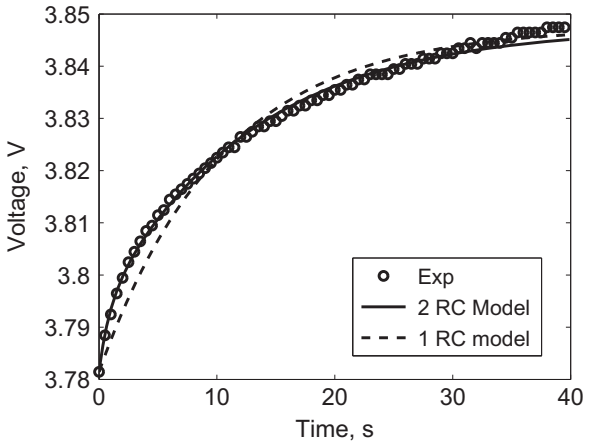

Fig. 2. The model fit to HPPC rest data.

of an electrode particle and its maximum value, C the electrolyte concentration, F is the Faraday's constant, R_G is the ideal gas constant, T is the absolute temperature, and the transfer coefficients α_a, α_c are taken typically to be 0.5.

At the onset of rest although the external current is zero, the charge transfer reaction continues to proceed by depleting the electrical double layer. The voltage continues to change till it reaches V_0, when the driving force for the reaction, the overpotential, becomes zero. The electric analog to this process is the self-discharge of the capacitor C_1 through R_1. Going back to Eq. (1) it can be seen that

$$I = 0 \quad \& \quad V = V_0 \Rightarrow \sum_n V_n = 0 \Rightarrow V_n = 0 \tag{14}$$

Thus the overpotential becoming zero is represented by V_1 becoming zero, thus identifying the V_1 to be overpotential for the charge transfer process. The Butler–Volmer equation is rewritten as follows:

$$i = i_0\left[\exp\left(\frac{FV_1}{2R_GT}\right) - \exp\left(-\frac{FV_1}{2R_GT}\right)\right] \tag{15}$$

The above equation is simplified as

$$i = 2i_0 \sin h(\eta); \quad \eta = \frac{FV_1}{2R_GT} \tag{16}$$

The derivative of the charge transfer current i wrt η gives

$$\frac{\partial i}{\partial \eta} = 2i_0 \cos h(\eta); \tag{17}$$

From the equation above, the form for R_1 is obtained as

$$R_1 = \frac{\partial V_1}{\partial i} = \frac{\partial \eta}{\partial i} \times \frac{2R_GT}{F} = \frac{r_{10}}{\cos h(\eta)}; \quad r_{10} = \frac{R_GT}{i_0F} \tag{18}$$

The analytical form for the charge transfer resistance derived from the Butler–Volmer equation is a variable resistor and is a function of V_1, the overpotential or the voltage drop across R_1. The observation that the cell can be modeled with variable resistors that are functions of the overpotentials is the key to further development of the model. Note also that r_{10} and η have built-in temperature dependences. This feature will be useful when a non-isothermal state space model is implemented. Typically the electric double layer processes [9] are considered to be parallel to the charge transfer reaction and C_1 be identified with the same. In the present work, this parameter is considered to be a constant.

5. Variable resistor model for diffusion and the high frequency resistance

In the previous section the equivalent resistance of a charge transfer reaction is derived. Here the theoretical forms for R and R_2 are developed. In the proposed model, the charge transfer reaction and double layer processes are represented by R_1C_1. The electronic and ionic conduction processes are represented by R. The remaining process of solid state diffusion is represented by R_2C_2. The equivalent resistance of diffusion in time domain is not uniquely represented in literature. It is represented as a series of RC pairs [9] or a transmission line [27]. It is known that the solid phase diffusivity varies with concentration [28]. Since the overpotential voltage is the state variable, this concentration dependence could be represented as voltage dependence. In this work, the equivalent resistance of diffusion (R_2) is represented by a variable resistor and C_2 is kept a constant. A general form of a variable resistor has a nonlinear voltage current relationship as given below:

$$I = \kappa |V|^{\alpha} \tag{19}$$

From this relationship, one can obtain the derivative of current wrt voltage as

$$\frac{\partial I}{\partial V} = \kappa\alpha |V|^{\alpha - 1} \tag{20}$$

and eventually the form for the variable resistance is obtained as

$$R_{\text{var}} = \frac{\partial V}{\partial I} = \frac{1}{\kappa\alpha}|V|^{1-\alpha} = R_{\text{var}}(V) \tag{21}$$

Rewriting Eq. (21) in terms of the overpotential V_2 the resistor R_2 is expressed in terms of two parameters r_{20}, and r_{21} as

$$R_2 = r_{20}|V_2|^{1-r_{21}} \tag{22}$$

Similar to the usage of Zener diode [29] and CPE in nonlinear equivalent circuit approaches [9], Eq. (22) represents the equation of a variable resistor or 'varistor' element. The 'high frequency' resistor R of the 2 pair RC model (Fig. 1) is typically identified with the electronic conductivity of the electrodes or the ionic conductivity of the electrolyte, or the contact resistances. Spectroscopy studies on $LiMn_2O_4$ spinels [30], one of the components of the cathode of the commercial cells, have shown that the electronic conductivity can change depending on the degree of intercalation. Also the ionic conductivity depends on the concentration of the electrolyte [26] that changes during cell discharge/charge. Both these results indicate that the high frequency resistor R can also be modeled as a 'variable resistor'. Here R is represented in terms of the cell voltage V with two parameters r_0, and r_1 as

$$R = r_0|V|^{1-r_1} \tag{23}$$

6. The state space model framework

A nonlinear state space model in the continuous time domain can be formulated [14,17,18,20] as follows:

$$\dot{x}(t) = f(x, u) \tag{24}$$

$$y(t) = g(x, u) \tag{25}$$

where x is the state vector, u is the input vector, y is the output vector, f and g are some nonlinear functions. Equation (24) is the state evolution equation and Eq. (25) is the output equation. In the proposed model, the individual RC pair voltages are the state variables, the current balance (Eq. (5)) is the state evolution equation and the voltage balance (Eq. (1)) is the output equation. Thus, $x = [V_1 \cdot V_2]$, $y = V$ and $u = I$, and the state evolution and output equations are written as

$$\begin{bmatrix} dV_1/dt \\ dV_2/dt \end{bmatrix} = \begin{bmatrix} -1/R_1C_1 & 0 \\ 0 & -1/R_2C_2 \end{bmatrix} \begin{bmatrix} V_1 \\ V_2 \end{bmatrix} + \begin{bmatrix} 1/C_1 \\ 1/C_2 \end{bmatrix} I \tag{26}$$

$$V = V_0 + IR + V_1 + V_2 \tag{27}$$

where R, R_1 and R_2 are obtained from Eqs. (18), (22) and (23) respectively, and C_1 and C_2 are constants. For a cell starting from an equilibrium state, for any process with known $I(t)$, the state evolution equations (Eq. (26)) are solved with the initial values for V_1 and V_2 (Eq. (10)). Subsequently cell voltage is obtained solving the output equation (Eq. (27)). Note that with R itself being a function of V, Eq. (27) is a transcendental equation in V, which is

solved numerically. V_0 appearing in the output equation (Eq. (27)) is obtained from the cell SOC. The cell SOC is computed from current history using

$$\mathrm{SOC} = \mathrm{SOC}_0 + \frac{1}{Q_{\max}} \int_0^t I dt \tag{28}$$

where $Q_{\max}$ is the maximum columbic capacity of the cell, SOC_0 corresponds to the initial capacity. With current being the input variable, this conforms to the state space formalism.

7. Cell experiments and equilibrium potential

The commercial cell based on which the model is developed consists of a composite of $LiNi_{1/3}Co_{1/3}Mn_{1/3}O_2$, $LiMn_2O_4$ as the cathode and MCMB as the anode. The multiple electrodes, electrolyte, and current collector assembly are enclosed in a pouch, resulting in a pouch cell. The cells have a capacity of about 15.3 Ah and nominal voltage of about 3.8 V. The data used for model development is obtained from the hybrid pulse power characterization (HPPC) test. In the HPPC test, the cell is discharged at a high constant current close to 7C rate for 10 s, rested at zero current for 40 s, and subsequently charged at the same constant current for 10 s. The sequence of pulse experiments, starting from a fully charged cell, is done at decreasing states of charge (SOCs) till the cell is fully discharged. The full HPPC cycle starts from a fully charged cell and a discharge at about 1C rate for 180 s results in the SOC reduction of around 5%. The cell is then equilibrated for 2 h, and the voltage at the end of this rest period is taken as the equilibrium potential V_0 at that capacity. (For modeling purposes at intermediate capacities this experimental data is interpolated.) Subsequently, the HPPC pulse as described above is conducted. After equilibration of around 360 s, steps from the 1C discharge are repeated till the end of discharge. Thus the HPPC cycle consists of discharge-rest-charge pulse at around 7C separated by 1C discharges and the equilibration periods in between.

The data used for model validation is obtained from full depth charge–discharge experiments. The full depth experiments are done at constant power (Ragone data), separated by constant current experiments. The constant current experiments are at 1C rate, whereas the constant power experiments are conducted at various rates, ranging from C/10 to 4C. All the HPPC tests are done at 30 °C and the full depth experiments at 25 °C.

8. Model implementation for HPPC data

The model consists of state evolution equation (Eq. (26)), output equation (Eq. (27)) with the initial voltage drops given by Eq. (10). The solution of the ODEs, the error minimization, and the solution of nonlinear equations are done in Matlab®. The expressions for R, R_1 and R_2 contain the five parameters $\{r_0, r_1, r_{10}, r_{20}, r_{21}\}$. The two capacitances C_1 and C_2 are the other two constant parameters. Thus this model has 7 parameters.

An HPPC pulse at any initial SOC consists of discharge, rest and charge. The model is applied to the HPPC data in two stages. In the first stage, the parameters are extracted from HPPC pulse data at a few SOCs, and the predictions are compared with experimental voltage at other SOCs, resulting in a global parameter set. In the second stage, the global parameter set from the first stage is used to predict the full HPPC protocol. The first and second stages demonstrate the predictability of the model.

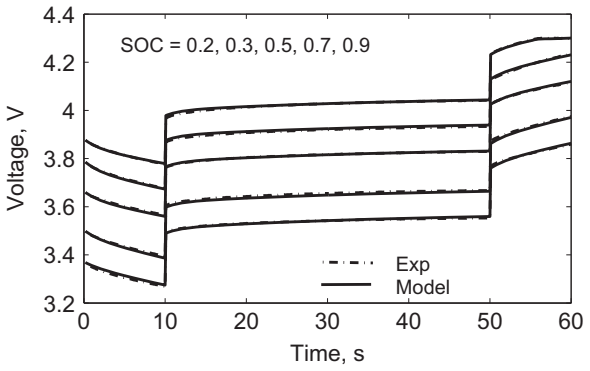

Fig. 3. Parameter extraction using HPPC data.

8.1. Results with global parameters

The first stage of implementation is to study the ability of the model to represent the HPPC pulse as well as the predictability of the model. To this end, HPPC data at five SOCs from 0.2 to 0.9 is chosen and a single set of 7 parameters is extracted by minimizing the root mean square error (RMSE) between the model output and the experimental voltage. The RMSE is defined by

$$\mathrm{RMSE} = \sum_{j=1}^{N} \sqrt{\frac{(V_{\mathrm{exp}} - V_{\mathrm{model}})^2}{N}}, \tag{29}$$

Fig. 3 shows that the model matches well with the experimental results at these chosen SOCs. This parameter set henceforth called global parameters is given in Table 1. The ability of the model to predict the cell voltages at other SOCs is tested, using *only* the initial value of the cell voltage at the respective SOCs. Fig. 4 is the model prediction at SOCs below 0.5. It shows good match for discharge, rest and charge processes at all SOCs. The model predictions of HPPC pulses at SOCs higher than 0.5 is also comparable (not shown). Fig. 5 shows the model predictions for SOCs outside the range 0.2–0.9, using which the global parameters are extracted, demonstrating the extrapolation capability of the model. The model prediction of all the processes at SOC 0.95 is good. There is an under-prediction during the end of discharge and beginning of charge at the very low SOCs, which deteriorates at lower SOCs. However, for all the HPPC pulses studied the maximum error between the model and experiments is less than 50 mV.

8.2. Prediction of the HPPC protocol

The entire HPPC protocol runs for about 44 h, with measurements accounting to 30,000 data points. The protocol consists of HPPC pulse (discharge, rest and charge) at different SOCs, interspersed with the SOC reducing discharges and equilibration, as explained above. The model is used to predict this HPPC protocol,

Table 1
Global parameters of the model.

Parameter	Value
r_{10}	0.00022062
C_1	8009.3
r_{20}	0.002211
r_{21}	1.0029
C_2	13,825
r_0	0.0038741
r_1	1.5406

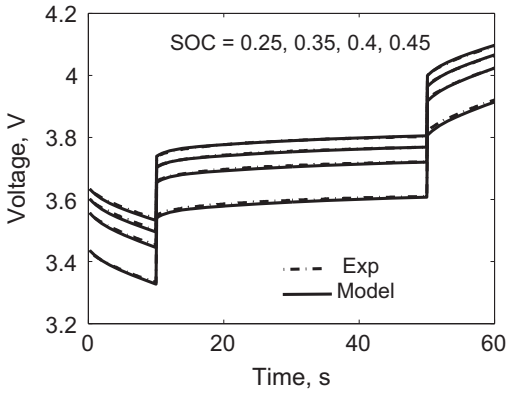

Fig. 4. Model prediction of HPPC data at SOC below 0.5.

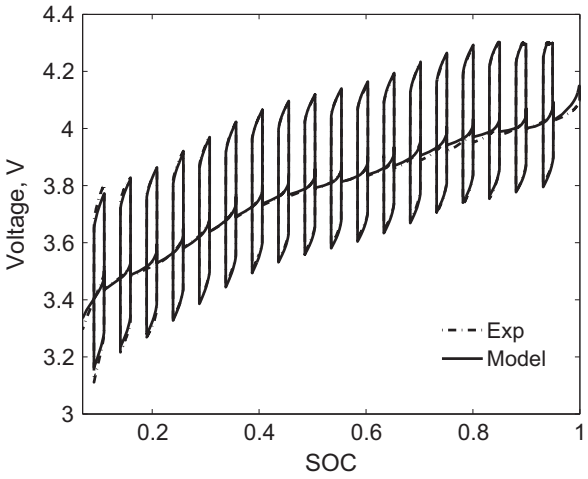

Fig. 6. Model prediction of the full HPPC cycle as a function of SOC. The experiment starts with the fully charged cell at SOC = 1.

from the fully charged cell to the fully emptied, using the global parameters in Table 1, with the fully charged cell voltage as the initial condition. The model predictions are compared with the experimental voltage in Fig. 6.

In Fig. 6, the voltage is plotted against SOC instead of time, because the 2 h equilibration periods occupy most of the total protocol than the HPPC pulses which last only for 60 s. The error in voltage prediction is plotted in Fig. 7. The model prediction is good for the entire SOC range from 1 to 0.06 with error less than 50 mV. The HPPC protocol has rapid transients akin to a real drive cycle, and the model predicts these transients reasonably well. Note that the HPPC pulse data used for parameter extraction has high current charge/discharge (105 A), whereas the SOC reducing discharges are at a low current (15 A). The model predictions are good at these SOC reducing discharges, demonstrating the robustness of the model construction, although there is no explicit current dependence built in the model. Thus, with a 7-parameter physics-based closure, the HPPC protocol over the entire SOC range is well predicted by the model.

8.3. Insights from the model predictions

The state space model can be used to resolve the overall cell potential into the potential drops due to individual processes, thereby yielding insights into the controlling mechanism. In Fig. 8, the resistances R, R_1 and R_2 are plotted as a function of time for a HPPC pulse at SOC around 0.5. Note that R and R_2 are nearly of same order of magnitude, and R_1 is one order of magnitude lower. In Fig. 9, the total overpotential, defined as $V–V_0$, is plotted as a function of time, along with the potential drops across the resistors R, R_1 and R_2. It shows that during the HPPC pulse at 30 °C, contribution to overpotential is predominantly due to the IR term, followed by the diffusion element, with a minor contribution from the reaction term. It is to be noted that during rest the IR contribution is zero, and the overpotential is mostly contributed by the diffusion element. Ideally experiments like impedance analysis are used to get insights about the controlling processes, since a frequency domain analysis separates the processes which are confounded in the time domain. However, with the state space model applied on a time domain data (HPPC pulse) qualitative inferences about the contributions of individual processes can be extracted.

It is seen from Fig. 8 that R is comparable with R_2, however, in Fig. 9 it is seen that during charge and discharge the magnitude of IR is higher than that of V_2. This behavior could be understood by resolving the current through R_2 and C_2, as in Fig. 10. The current through R_2 is $I_{R_2} = V_2/R_2$ and the current through C_2 is $I - I_{R_2}$. It is seen from Fig. 10 that at even 10 s, the end of the discharge period, a significant part of the total current flows through the capacitor C_2. The capacitor is not fully charged during the discharge period of 10 s, since its average time constant $\tau_2 = R_2C_2$ is about 30 s. Since the current splits significantly between R_2 and C_2 branches, the potential drop V_2 is significantly lower than the IR drop, where the entire current passes through R. This observation shows that the transient potential drop across a resistive element in an RC pair could be reduced significantly by increasing the parallel

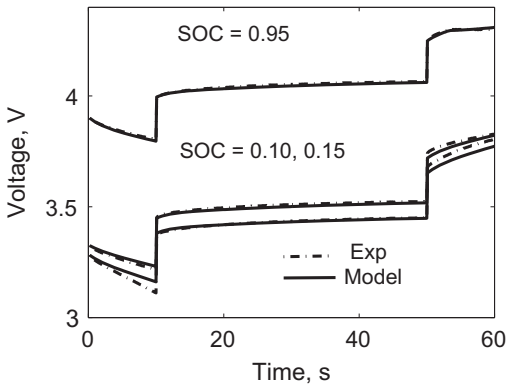

Fig. 5. Model prediction at SOCs outside the data used for parameter extraction.

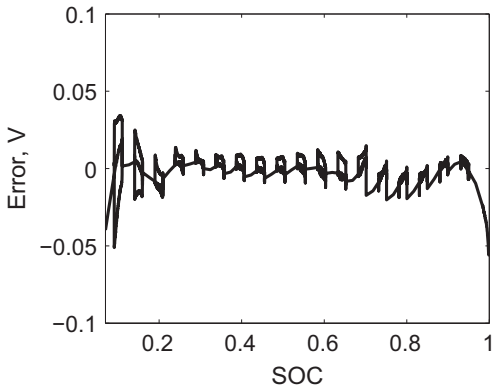

Fig. 7. Error model in prediction of the full HPPC cycle.

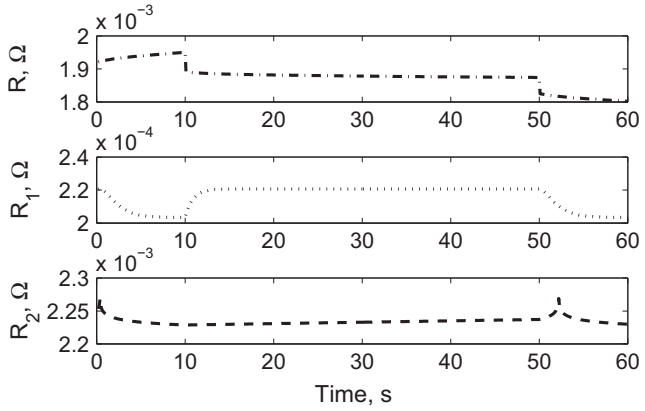

Fig. 8. The values of R, R_1 and R_2.

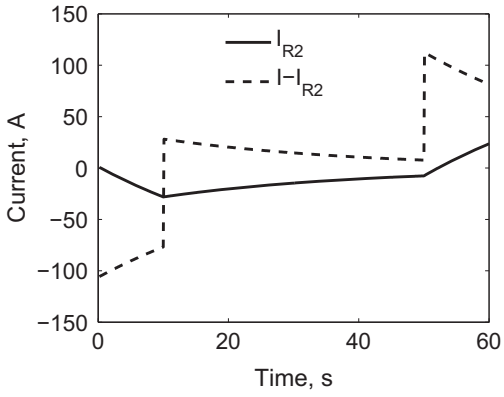

Fig. 10. The individual contributions of diffusion resistance and the capacitance terms.

capacitance. Thus, a higher parallel capacitance will lead to slower response and lower potential drop, and a lower parallel capacitance will lead to faster response and higher potential drop.

Analysis of Fig. 8 brings forth an important feature of the variable resistor formalism that could be particularly useful for on-board applications. It is seen that the resistors R, R_1 and R_2 change continuously throughout the duration of the HPPC pulse. This variation is accomplished with the same values of model parameters $\{r_0, r_1, r_{10}, r_{20}, r_{21}\}$, due to the proposed functional dependences (Eqs. (18), (22) and (23)) on the voltage or overpotential. For an on-board scenario specified by a drive profile current I, the corresponding overpotentials can be obtained by solving Eq. (26). The resistors R_1 and R_2 can simultaneously be computed from Eqs. (18) and (22), and the cell voltage obtained by solving Eq. (27) with Eq. (23). Thus the variable resistor formalism enables on-board voltage prediction without any parameter re-estimation.

The present model is isothermal at this stage. In order to make this approach applicable to actual driving scenarios, the temperature dependence of the parameters need to be built in. Also, as the cell ages, the parameters will change, necessitating a re-estimation while on-board. These developments are currently under progress.

9. Model validation with full depth charge–discharge data

The HPPC protocol has high current charge–discharge HPPC pulses and rest period where current is zero. Such constant current data at few SOCs is used to extract the global parameters, and tested the predictions of HPPC pulses at other SOCs and the low current discharges used for SOC reduction. The state space model is validated using the global parameters obtained from the HPPC data to predict the full depth charge–discharge data which includes the constant power or Ragone process as well as constant current process. During the Ragone process, since power is constant, current varies continuously offering a different scenario from the HPPC protocol which had only constant current sections. Mathematically, in the evolution equation of the state variables (Eq. (26)), the external current forming the non-homogeneous term becomes a time dependent term in Ragone process, while it was a constant or zero during the HPPC protocol. Also during Ragone process, the capacity varies continuously as opposed to the HPPC protocol. Hence, it offers a meaningful scenario for model validation. The data used for validation is generated at 25 °C. V_0 is obtained from equilibration region of the HPPC experiments conducted at the same temperature.

The model comparisons of voltage for discharge experiments are plotted in Fig. 11 as a function of the discharge time, at various discharge rates. The model predicts the experimental voltage accurately for most regimes of discharge. A mismatch is seen near the end of discharge and is higher at higher rates, probably due to uncertainty in initial capacity estimation. The model also matches well with the experiments for both constant current and constant power charge (results not shown) except that a slight mismatch is observed at the initial regimes of charge at high rates.

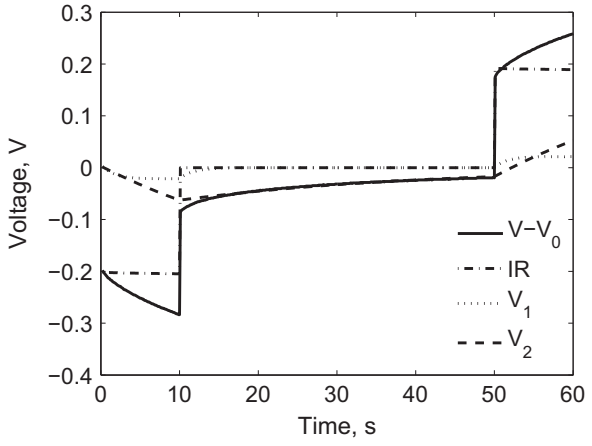

Fig. 9. Contributions to the total overpotential by various processes for the HPPC pulse around SOC 0.5.

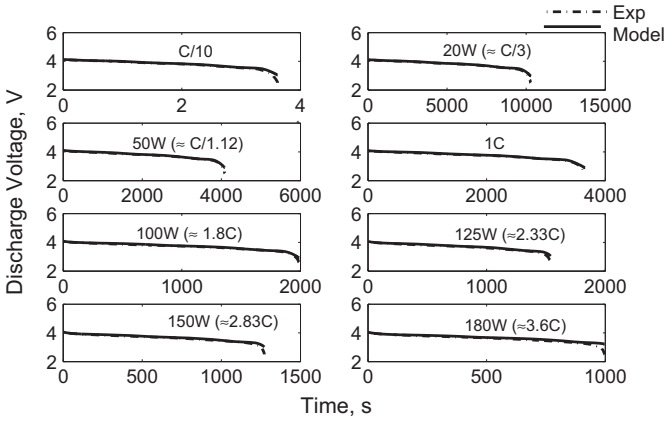

Fig. 11. Model prediction of full depth constant power (Ragone) and constant current discharge data at various rates.

10. Summary and conclusions

A nonlinear equivalent circuit model is developed where the circuit elements are based on electrochemical processes like the charge transfer reaction and variable resistances. It is found that the overpotential, or the potential drops are natural state variables rather than a cell level state-of-charge. Using HPPC rest data it is shown that a two pair RC circuit is the minimal equivalent circuit required for the commercial cells under study at 30 °C. The state space model consists of the current balance which forms the state variable evolution equation and the voltage balance which forms the output equation. A global set of parameters is calculated by solving the model equations consistently and minimizing the error with HPPC pulse voltage at few SOCs and used to predict the HPPC pulse voltage at other SOCs. The entire HPPC protocol, which goes from a fully charged to fully discharged state, is predicted by the model accurately within an error of 50 mV. The model is validated using the full depth charge–discharge experiments. The state space model is used to resolve the overall cell potential into potential drops due to ionic/electronic conductivity, charge transfer reactions and solid phase diffusions, thereby yielding insights into the controlling mechanism. The model is used to resolve the total current flow between the resistive and capacitive branches, and infer the effect of this split on the total potential drop. As the variable resistor formalism enables cell voltage prediction without parameter re-estimation under normal operating scenarios; on-board algorithms are expected to be simpler than the conventional SOC based ad hoc closures. State space approach to equivalent circuit models is quite promising by virtue of its rigorous formulation, elegant solution methodology and ease of on-board integration.

In future the state space model implementation will be extended across the entire temperature range of cell operation. In the current work the variable resistor model is used for the equivalent resistance of solid phase diffusion process. In future it will be replaced with a rigorous electrical analog. The current state space model implementation is for the full cell experimental data. Note that the equivalent resistances of reaction and diffusion represent these processes occurring in both the electrodes. However, once the half cell experimental data is available, the present formalism could be applied independently to anode and cathode data, generating an equivalent circuit model for the individual electrodes. These two models could then be combined to obtain the overall cell model. Such a dual electrode model is expected to give deeper insights into the individual electrode processes, and hence give better predictions when control mechanisms shift from one electrode to another.

Acknowledgments

The authors like to acknowledge Brain Koch, Vehicle Electrical Center and Ramona Ying, Research and Development Center, General Motors Corporation, Warren, Michigan 48090-9055, USA for the data on the commercial cells.

List of symbols

SOC	cell state-of-charge
V_0	cell equilibrium potential, V
V	cell voltage, V
I	cell current, A
V_n	voltage drop across nth RC pair, V
R_{var}	general expression for a variable resistance, ohm
R	high frequency resistance, ohm
R_1	resistance representing the charge transfer reaction, ohm
R_2	resistance representing the solid phase diffusion, ohm
C_1	capacitance representing the double layer, F
C_2	capacitance representing the solid phase diffusion, F
Q_{max}	maximum Columbic capacity of the cell, A h

References

[1] T. Miller, Advances in NiMH and Li-ion batteries for full hybrids, in: Advanced Automotive Batteries Conference, Baltimore, 2006.
[2] K.-W. Nam, W.-S. Yoon, H. Shin, K.Y. Chung, S. Choi, X.-Q. Yang, J. Power Sourc. 192 (2009) 652–659.
[3] P. Albertus, J. Christensen, J. Newman, J. Electrochem. Soc. 156 (2009) A606–A618.
[4] M.W. Verbrugge, R.Y. Ying, J. Electrochem. Soc. 154 (2007) A949–A956.
[5] M.W. Verbrugge, R.S. Conell, J. Electrochem. Soc. 149 (2002) A45–A53.
[6] P.L. Moss, G. Au, E.J. Plichta, J.P. Zheng, J. Electrochem. Soc. 155 (2008) A986–A994.
[7] M. Chen, G.A. Rincón-Mora, IEEE Trans. Energy Convers. 21 (2006) 504–511.
[8] E.B. Castro, D.J. Cuscueta, R.H. Milocco, A.A. Ghilarducci, H.R. Salva, Int. J. Hydrogen Energy 35 (2010) 5991–5998.
[9] S. Buller, Ph.D. dissertation, ISEA, RWTH Aachen, Aachen, Germany, 2003.
[10] S. Buller, M. Thele, E. Karden, R.W. De Doncker, J. Power Sourc. 113 (2003) 422–430.
[11] P. Mauracher, E. Karden, J. Power Sourc. 67 (1997) 69–84.
[12] E. Barsoukov, J.H. Kim, C.O. Yoon, H. Lee, J. Power Sourc. 83 (1999) 61–70.
[13] M. Pasquali, A. Dell'Era, P.P. Prosini, J. Solid State Electrochem. 13 (2009) 1859–1865.
[14] C.P. Zhang, J.Z. Liu, S.M. Sharkh, C.N. Zhang, in: International Symposium on Electric Vehicles (ISEV), Beijing, China, 2009.
[15] J. Lee, O. Nam, B.H. Cho, J. Power Sourc. 174 (2007) 9–15.
[16] S. Lee, J. Kim, J. Lee, B.H. Cho, J. Power Sourc. 185 (2008) 1367–1373.
[17] J. Chiasson, B. Vairamohan, IEEE Trans. Control Sys. Technol. 13 (2005) 465–470.
[18] S. Pang, J. Farrell, J. Du, M. Barth, in: Proc. Amer. Control Conf., vol. 2, 2001, pp. 1644–1649.
[19] W. Liu, M.J. Gielniak, J. Lin, B.J. Koch, D.R. Frisch, J.M. Lograsso, US patent, 20100076704.
[20] G.L. Plett, J. Power Sourc. 134 (2004) 262–276.
[21] V.H. Johnson, A.A. Pesaran, T. Sack, in: 17th Annual Electric Vehicle Symposium, Montreal, Canada, 2000.
[22] S. Santhanagopalan, R.E. White, J. Power Sourc. 161 (2006) 1346–1355.
[23] D.D. Domenico, G. Fiengo, A. Stefanopoulou, in: 17th IEEE Intl. Conf. Control Appl., Texas, USA, 2008.
[24] K.A. Smith, C.D. Rahn, C.-Y. Wang, IEEE Trans. Control Sys. Technol. 18 (3) (2010) 654–663.
[25] Y.-H. Kao, M. Tang, N. Meethong, J. Bai, W.C. Carter, Y.-M. Chiang, Chem. Mater. 22 (2010) 5845–5855.
[26] M. Doyle, J. Newman, A.S. Gozdz, C.N. Schmutz, J.M. Tarascon, J. Electrochem. Soc. 143 (1996) 1890–1903.
[27] H.-M. Cho, Y.J. Park, H.-C. Shin, J. Electrochem. Soc. 157 (2010) A8–A18.
[28] M.W. Verbrugge, B.J. Koch, J. Electrochem. Soc. 150 (2003) A374–A384.
[29] S. Abu-Sharkh, D. Doerffel, J. Power Sourc. 130 (2004) 266–274.
[30] C.M. Julien, M. Massot, J. Phys. Condens. Mater. 15 (2003) 3151–3162.